Numerical simulation of the femur fracture for different cemented hip femoral prosthesis under forces during stumbling

MS. ZAGANE, A. SAHLI, A. BENOUIS, S. BENBAREK

LMPM, Department of Mechanical Engineering, University of Sidi Bel Abbes, BP 89, City Ben M'hidi, Sidi Bel Abbes 22000, Algeria, salah_cao@yahoo.fr

Résumé :

Prothèse totale de la hanche a été utilisé pour les patients qui a la fracture de la hanche et incapable de récupérer naturellement. Pour concevoir des prothèses très durables, il faut tenir compte des processus naturels qui se produisent dans l'os. Dans ce papier, l'analyse de charge statique est basée, en sélectionnant la charge de pointe pendant l'activité de trébuchement. Deux matériaux d'implant différents ont été sélectionnés pour étudier le matériel approprié. Les résultats ont montré la différence du maximum de Von Misses et ont détecté la fracture du fémur pour différents modèles (Charnley et Osteal) avec la méthode des éléments finis étendus (X-FEM) et après les résultats de la simulation numérique de X-FEM pour différent a été utilisé dans la détermination des facteurs d'intensité de contrainte (SIF) pour identifier les matériaux d'implant de comportement de fissure pour différentes longueurs de fissures. Il a été montré que les facteurs d'intensité de contrainte maximale ont été observés dans le modèle de Charnley.

Abstract :

Hip total prosthesis was used for the patients who has the hip fracture and unable to recover naturally. To design highly durable prostheses one has to take into account the natural processes occurring in the bone. In this paper, the static load analysis is based, by selecting the peak load during the stumbling activity. Two different implant materials have been selected to study appropriate material. The results showed the difference of maximum von Misses stress and detected the fracture of the femur shaft for different model (Charnley and Osteal) implant with the extended finite element method (X-FEM), and after the results of the numerical simulation of X-FEM for different was used in determining the stress intensity factors (SIF) to identify the crack behavior implant materials for different crack length. It has been shown that the maximum stress intensity factors were observed in the model of Charnley.

Mots clefs : Prothèse totale de la hanche (PTH); Méthode des éléments finis étendus (X-FEM); Fracture de l'os; Fémur; Trébuchant; Facteur d'intensité de contrainte (FIC).

1 Introduction

Total Hip Prosthesis (THP) is an excellent alternative for patients suffering from arthritis or hip fracture [1,2]. Millions of people undergo total hip replacement every year [3]. To avoid injuries and fractures of the femur (cortical bone cement, implant) in patients after the replacement THP, surgeons need published information about the clinical results of different joint replacements; However, many important factors are still very difficult to take into account during these studies. In particular, these aspects related to the patient (skeletal anatomy, bone quality, muscles, level of activity or biological response) or to the surgeon (bone surgery, implant position and fit, joint center relocation or muscle surgery). El'Sheikh et al, compared the hip prosthesis component subjected to a dynamic stumbling load and the peak static load of the similar patient load behavior [4]. S. Shankae et al, to predict the impact of different material combination pairs on the acetabulam contact model during stumbling cycle to assess the contact stresses and deformation on the lines of our previous static model [5].

This study aims to evaluate the three dimensional (3D) finite element (FE) inlay retained and only supported partial models were established for use to examine the behavior of the hip total arthoplasty and cracks within the bone cortical with different types of the femoral implant: Charnley stem and the Osteal stem. The Charnley and Osteal hip prostheses are both cemented, but have different head sizes and different femoral stem profiles. The Charnley femoral component has a more bulky cross section than the Osteal component, but the latter is designed to be placed centrally in the femoral canal when the neck cut is correct to facilitate a symmetrical cement mantle (Fig. 1).

Bone femoral fracture models were predicted using the extended finite element method (X-FEM) which enriches the FE approximation space with special functions that introduce the displacement discontinuity across the crack faces and the singular behavior associated with the crack front, and makes its analysis, up to a certain point, independent of the mesh [6,7].

Numerous previous studies have been devoted to analysis of quasi-static mechanical properties and resistance to fracture of the cortical bone tissue have implemented X-FEM For instance, Adel, A. Abdel-Wahab, a two-dimensional numerical (finite-element) fracture model for osteonal bovine cortical bone was developed to account for its microstructure using extended finite element method (X-FEM) [8]. Another study, by Bonney et al, was devoted to investigation of local variations in mechanical properties of cortical bone (porcine femur) [9].

In addition, Simin, Li. et al to develop a finite-element approach to evaluate the fracture process in cortical bone at micro-scale**)** [10]. For instance, Budyn and Hoc introduced a multiscale method to simulate multiple crack growth in a cortical bone tissue using X-FEM under simplified tensile loading conditions [11]. In another recent attempt, Liu et al developed a homogenised X-FEM model to predict fracture of a proximal femur due to impact [12].

The extended finite element method (X-FEM) has emerged as a powerful tool to analyse cracks and measuring SIF [13]. Is an important parameter, which judges whether there is crack propagation. So, the numerical evaluation of the SIF is an important issue in applied fracture mechanics [14]. Guian Qian et al to compare different numerical methods for mode I stress intensity factor (SIF) calculations [15]. Using the finite element method (FEM) and extended finite element method (X-FEM). X-FEM method shows advantages in modeling cracks, but oscillations in 3D.

After analysis of comparisons of predicted and fracture patterns for different model (Charnley and Osteal) implant under the forces during stumbling and show the von Misses stress distribution on the hip prosthesis total.

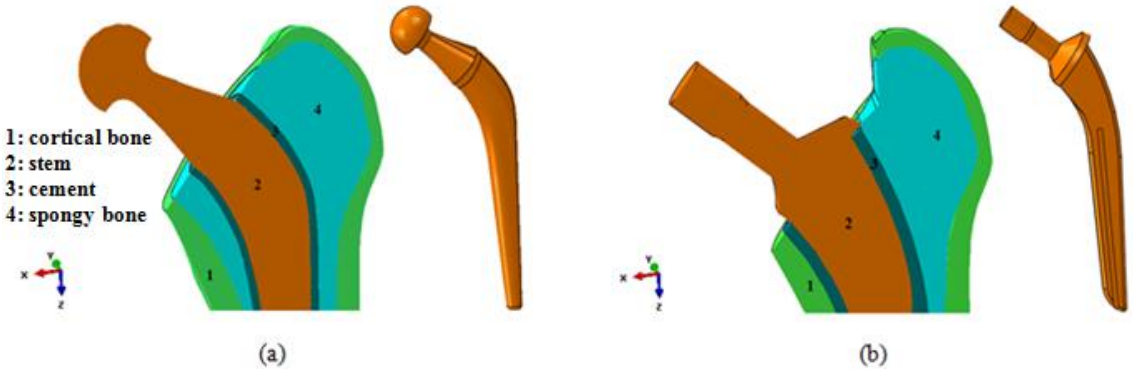

Fig. 1 Three-dimensional Femur stems for two models. (a): Charnley model (b): Osteal model

2 Finite element model

The 3D FE models the femur, cement layer and femoral prosthesis were meshed by four nodes, tetrahedral element (C3D4). The femur, bone cement and Charnley prosthesis were divided into 855 583, 88811, and 229 065 elements, respectively, in the smallest mesh size. The complete Charnley model (stem, bone cement and femur) has in total 1173459 elements. Are shown in Fig.2.a and model of Osteal. The femur, cement and the femoral prosthesis were divided into 925 543, 92 851 and 329 065 elements, respectively, The complete Osteal model (stem, bone cement and femur) has in total 1347459 elements. Are shown in Fig.2.b.

Fig. 2 Finite element meshes of hip prosthesis components

3 Material Properties

The mechanical properties of the materials are presented in Table1. The cortical bone was considered a transversely isotropic elastic material, whereas the spongy bone, cement, Charnley stem stainless steel 316 L, and Osteal stem Ti-6Al4V were considered linear isotropic elastic materials. To assign material properties of the cortical bone, elastic properties were inserted into ABAQUS 6.13.

Materials	Young's modulus E (Gpa)	Poisson ratio υ	Yield Strength (Gpa)	Ultimate Tensile Strength (Gpa)	Reference
Charnley stem stainless steel 316 L	230	0.3	0.455	0.65	(2006)

Osteal stem Ti-6Al4V	110	0.3	0.795	0.86	[16,17,18]
Cortical bone	17	0.36	0.16	0.035	[19]
Bone Cement	2	0.38	0,0438	0.0353	[20,21]
Cancellous Bone	0.5	0.3	0.00389	-	[20,21]

4 Loading Condition

In this study, the magnitudes and the directions of muscle force data by Bregmann [21]. An abductor muscle load $F_{abductor}$ muscle is applied to the proximal area of the greater trochanter. An ilio tibial-tract load $F_{ilio\ tibial\text{-}tract}$ is applied to the bottom of the femur in the longitudinal femur direction is used. They are shown in (Table 2). Fig. 3 shows the coordinate system used to represent the direction of the forces components. The boundary condition was applied by fixing the distal epiphysis [23].

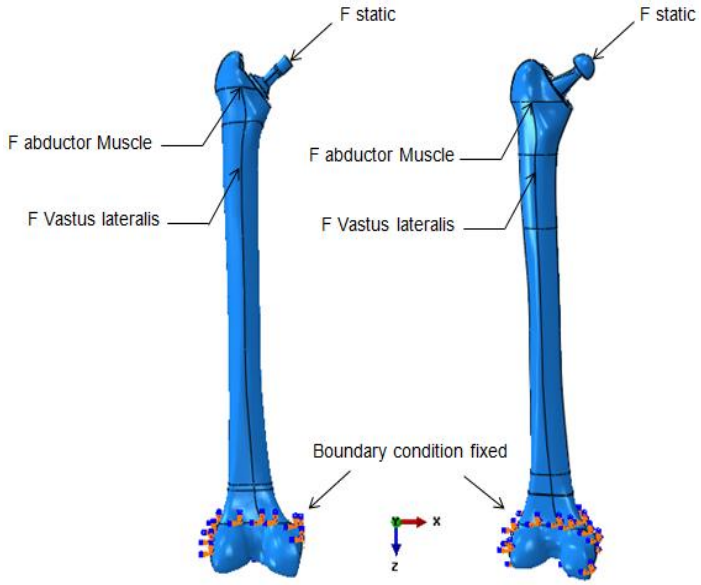

Fig. 3 Boundary conditions and the distribution of the applied and muscle forces on THP.

Table 2 Muscle load magnitudes applied to the FE model [21]**.**

Force	Fx (N)	Fy (N)	Fz (N)
Abductor	465.9	34.5	695.0
Vastus Lateralis	7.2	148.6	746.3

Optimum values of coefficient of friction, 0.4 for cement-stem and 1.0 for cement-bone interfaces, were considered respectively [24].

Table 3Contact details [24].

Femur head-Stem	Cancellous-Cortical	PMMA-Cancellous	Femur head-XLPE	Stem-PMMA
Bonded		Frictional contact (μ=1)	Frictional contact (μ=0.2)	Frictional contact (μ=0.4)

The loading applied was taken from the work of Bergman [22] it is illustrated in Fig. 4 which represent loading pattern for stumbling. In static analysis, the maximum force analysis was employed to simulate simplified loading on the implanted femur for stumbling activity, this load analysis is based, by selecting the peak load during the stumbling activity. Stumbling resultant force,F, on the head of the femur is 8.7 times the body weight (BW = 70 kg) at 58% of the gait cycle. This can be resolved into: Fx: -2053.02 (N) Fy: 613.77 (N) Fz: 5693.49 (N)

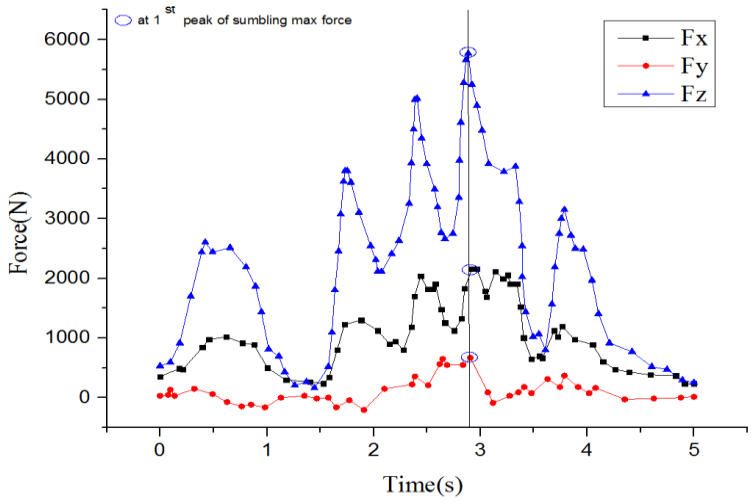

Fig. 4 The variation of forces applied on the prosthesis during stumbling [21].

5 Fracture criteria for X-FEM

The X-FEM was first introduced by Belytschko and Blackand, and then, it was employed by many researches to carry out their study in the field of fracture mechanics [25]. Extended finite element method (X-FEM) is the most effective numerical method to solve discrete mechanical problem. The X-FEM was applied to simulate crack initiation and propagation of the model, The basis for damage initiation as per the criterion of the maximum principal stress (σ_1) as indicated in Eq.1

$$f^e = \frac{\sigma_1^e}{<\sigma_{max}^*>} \quad (1)$$

The symbol < > represents the Macaulay bracket with the usual interpretation that is:

$$<\sigma_{max}^*> = 0 \text{ if } \sigma_1^e < 0$$

$$\text{And } <\sigma_{max}^*> = \sigma_1^e \text{ if } \sigma_1^e \geq 0$$

Compressive stress does not initiate the damage. When the boot fe ≥ 0 criteria is met. Developed in commercial finite element software-Abaqus [26]. The parameters required by the X-FEM for models were selected on the basis of experimental data from the literature table 4 [27].

Table 4 X-FEM damage parameters [27].

	Bone properties	
σ_{nc} (Mpa)	G_{nc} (N/mm)	G_{sc} (N/mm)
116	1.16	2.97

σ_{nc}: the normal strength; G_{nc}: fracture toughness for opening mode; G_{sc}: shear mode

5.1 Calculation of the stress intensity factor by X-FEM

X-FEM was mainly developed to compute discontinuous and singular problems and it also simplifies the modeling of cracked structures and components. Therefore, X-FEM can also be used for calculating SIF. The advantage of X-FEM lies in the crack modeling, because no remeshing is needed in the crack growth problems and the crack path can be calculated. Discontinuities can also be within elements. The essential idea of X-FEM is to use a displacement field approximation that can model any crack face discontinuity and the near crack-tip asymptotic stress field. As a consequence, it is not necessary to modify the mesh to consider a specific crack; at most, moderate refinement must be introduced around the crack to achieve good accuracy [6,7]. Furthermore, X-FEM has been implemented in the commercial FE code ABAQUS 2013.

The displacement approximation for the extended finite element formulation used for crack modeling takes the form:

$$U_{XFEM}(X) = \sum_{i\in I} Ni\,(X)H(X)ai + \sum_{i\in K}[Ni(X)\sum_{\alpha-1}^{4} F\alpha(X)bi\alpha] \quad (2)$$

Where I is the set of all nodes in the mesh, Ni(X) are the nodal shape function and we are the standard DOFs of node i (ui represents the physical nodal displacement for non-enriched nodes only). The subsets J and K contain the nodes enriched with the Generalized Heaviside function H(X) or the crack-tip .Functions $F\alpha(X)$, respectively, and ai, $b_{i\alpha}$ are the corresponding DOFs. Fig.5 shows the enrichment method in X-FEM. The nodal degrees of freedom corresponding to the displacement are i u , j a , k bα , Ni , Nj , Nk are the shape functions respectively. H (x) is the generalized Heaviside function which takes the value +1 if x is above the crack and -1 otherwise.

$$H\,(x) = \begin{cases} +1 \text{ above the crack} \\ -1 \text{ below the crack} \end{cases} \quad (3)$$

x α φ is the asymptotic crack-tip fields, which implies the discontinuity occurs at the location of the crack.

$$b_k^a = \left(\sqrt{r}\,\sin\frac{\theta}{2}, \sqrt{r}\,\cos\frac{\theta}{2}, \sqrt{r}\sin\theta\sin\frac{\theta}{2}, \sqrt{r}\sin\theta\cos\frac{\theta}{2}\right) \quad (4)$$

Where (r ,θ) is the local polar coordinates at the crack tip. Note that the first function in Eq. (4) is discontinuous across the crack faces where the last three functions are continuous.

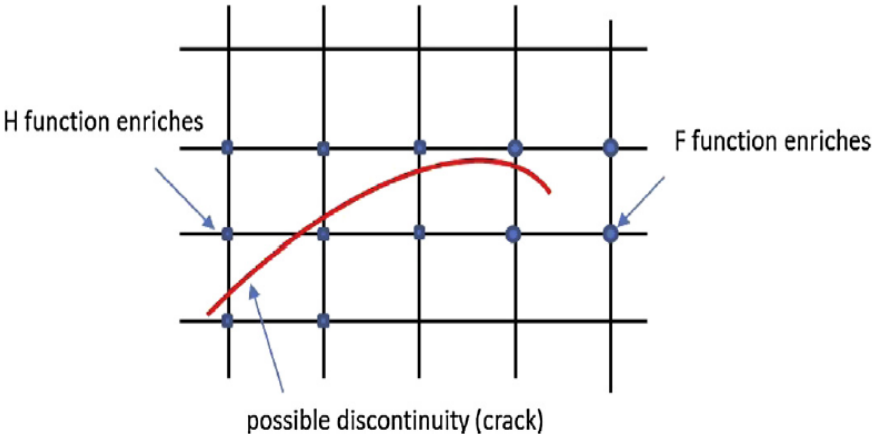

Fig. 5 Enrichment method in X-FEM.

The modeling of the damage is not automatically done by the software, it was assumed the existence of a crack and it has varied the languor of the latter for each languor and then it was calculated the factor intensity of constraint. To calculate the stress intensity factors (SIF) to identify the crack behavior implant materials for different crack length (2, 10 and 30 mm). The crack is located at the shaft femoral and its radius is defined in Fig. 6.

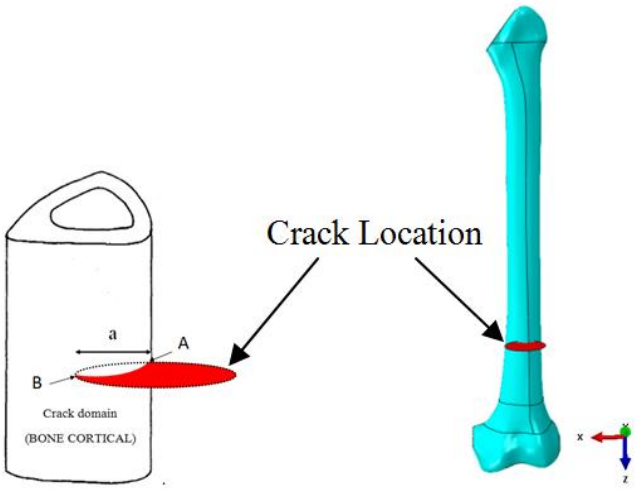

Fig. 6 Defining a crack for X-FEM.

The main advantage of the X-FEM besides the accuracy in predicting the crack growth path and fracture parameters is omission of special meshing for crack models in numerical analysis [28,29]. The X-FEM mesh, as shown in Fig. 7 (a) , is built with a regular linear hexahedrons 3D grid. A mesh adapted to the crack geometry can be used to minimize the calculation error in the X-FEM study. Fig. 7 (b) shows the mesh, adapted to the crack geometry.

 (a)	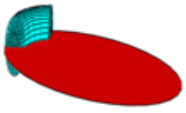 (b)	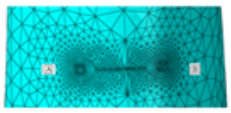 (c)	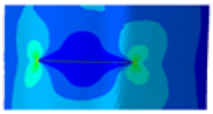 (d)
(a) mesh with X-FEM method with hexahedron elements,	(b) mesh with X-FEM with adapted mesh,	(c) mesh with FEM,	(d) Stress distributions for the model a curved crack model with X-FEM model.

Fig. 7 Meshes for model with curved crack.

6 Results and discussions

The stresses may occur as tensile, compressive, shear, or a stress combination known as equivalent Von Mises stresses. Von Mises stresses depend on the entire stress field and are a widely used indicator of the possibility of damage occurrence. Thus, Von Mises stress was chosen for presentation of results. The stress distribution was identified for each component of the hip prosthesis for Charnley and Osteal models. The values obtained of these stresses around the components of the prostheses are shown in Fig. 8.

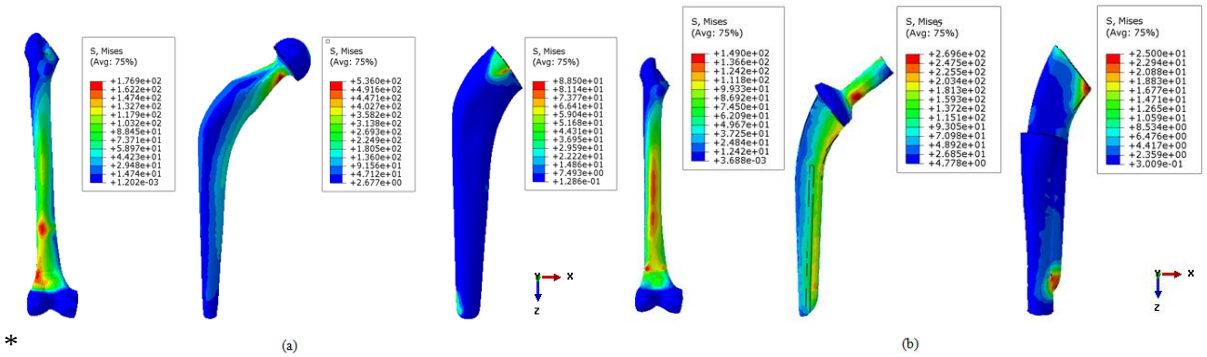

Fig. 8 Von Mises stresses in the hip prostheses components: stem, cement and femur bone. (a): Charnley model (b): Osteal model.

Comparing the stress distribution on the hip prostheses, it can be observed the stress concentration will be always at the neck area. Again, this is reasonable since there is a cross section transition at the neck area that it should always exhibit high stress. The maximum tensile stress being located in the middle of the lateral side of the prosthesis stem with a peak stresses almost equal (536 Mpa for Charnley model and 269.6 Mpa for Osteal model), For the comparison of stress distribution in the cement mantle The maximum stress is below 88.5 Mpa for Charnley model and 25 Mpa for Osteal model, in spite of the fact that the peak tensile stress for the Charnley model is greater than that of Osteal model one, it was localized in a small region in the inner interior side of the upper proximal part. For the femurs of the two models the maximum tensile stress exists in the distal part with a value of 176.9 Mpa which is greater than that for the Osteal model of 149 Mpa. By using the static analysis the treated femur expected to bend in the medial side showed resistance to the vertical applied load. As a result, the peak tensile stress is localized in the upper third of the lateral side, Fig. 9.

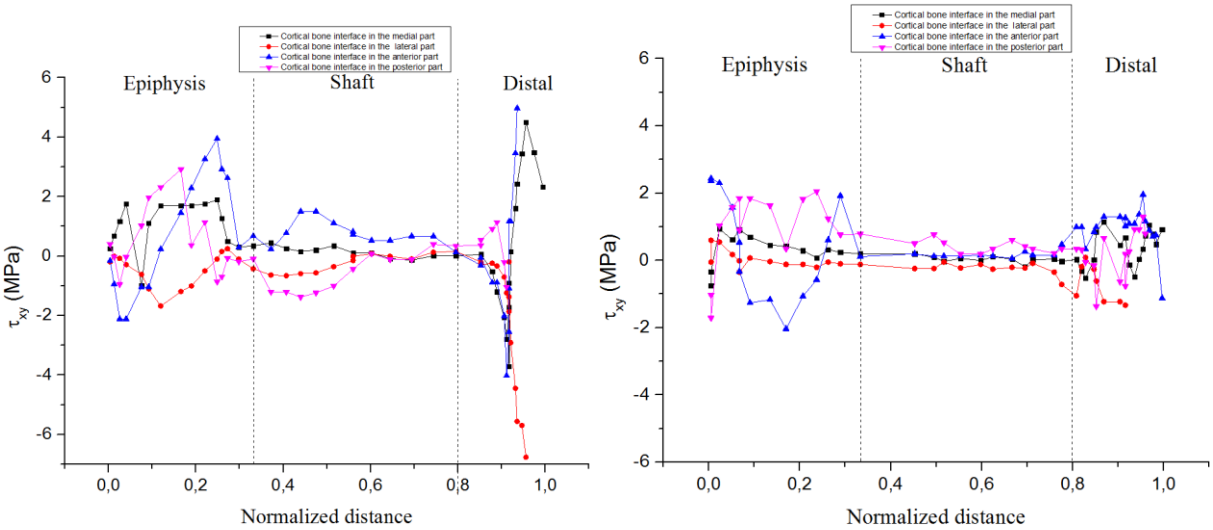

Fig. 9 Shear stresses along the different regions of the bone cortical. (a): Charnley model (b): Osteal model.

Figs. 9 show the variation of the shear stresses along the different regions of the cortical bone of the Charnley and Osteal prostheses. For Charnley prosthesis, the high value of shear stress in the cement mantle is observed at cortical bone interface, the maximum stress value is about 5 Mpa. For Osteal prosthesis, the maximum value of shear stress (2.5 Mpa) is localized in the epiphysis region at cortical bone.

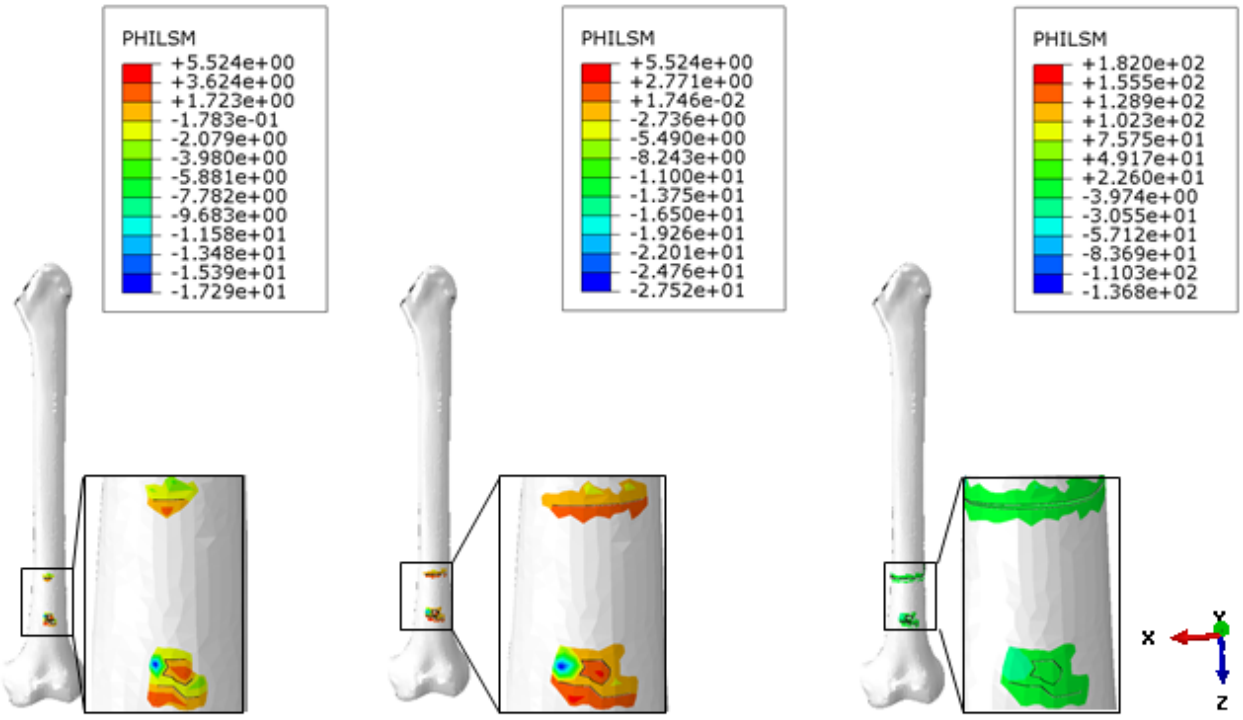

(a)

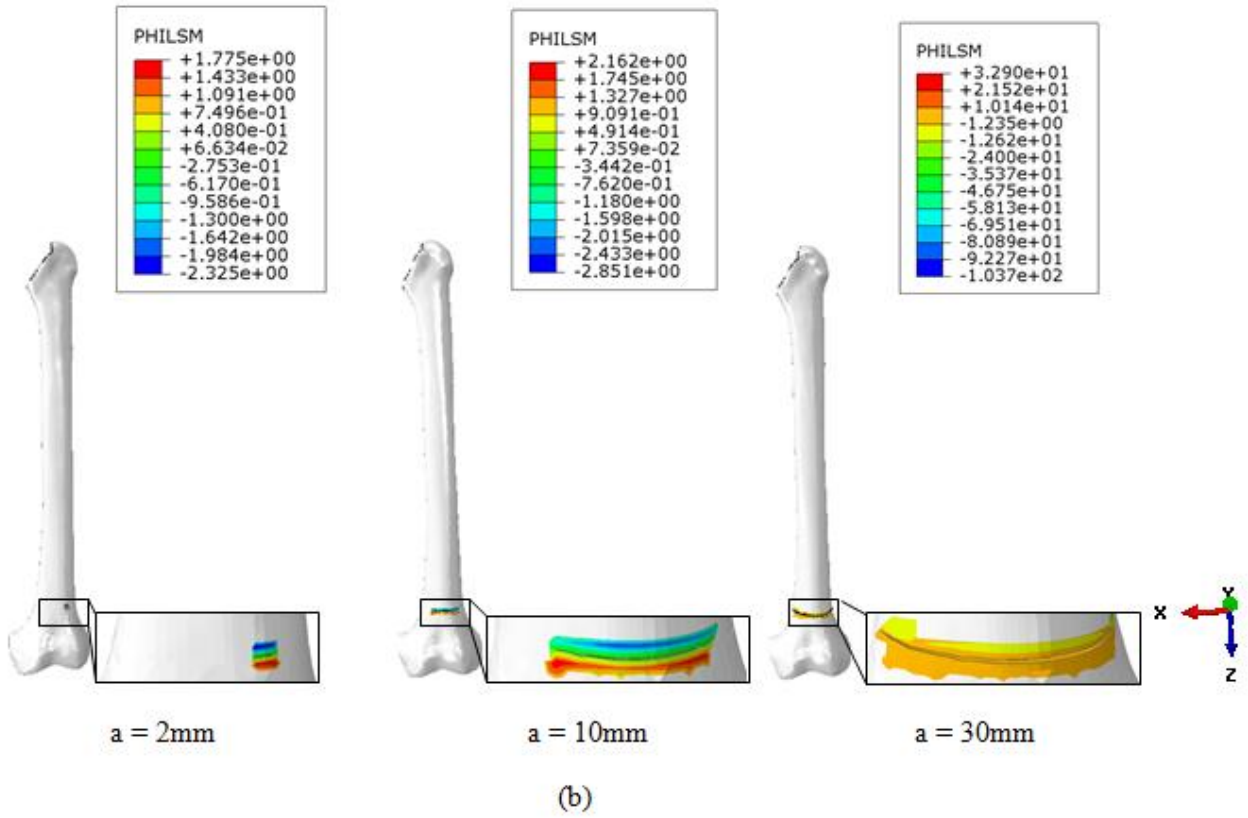

(b)

Fig. 10 X-FEM fractures patterns for the different prosthesis in the bone femoral. (a): Charnley model (b): Osteal model.

The figure. 10 show the simulation results with the X-FEM we detected the crack initiation and follow its propagation in the femur, the fractures propagate through the femoral shaft in its lower part flow third horizontal path in the shaft section for the two models (Charnley and Osteal implant) and resulting from the complete rupture of the shaft femur.

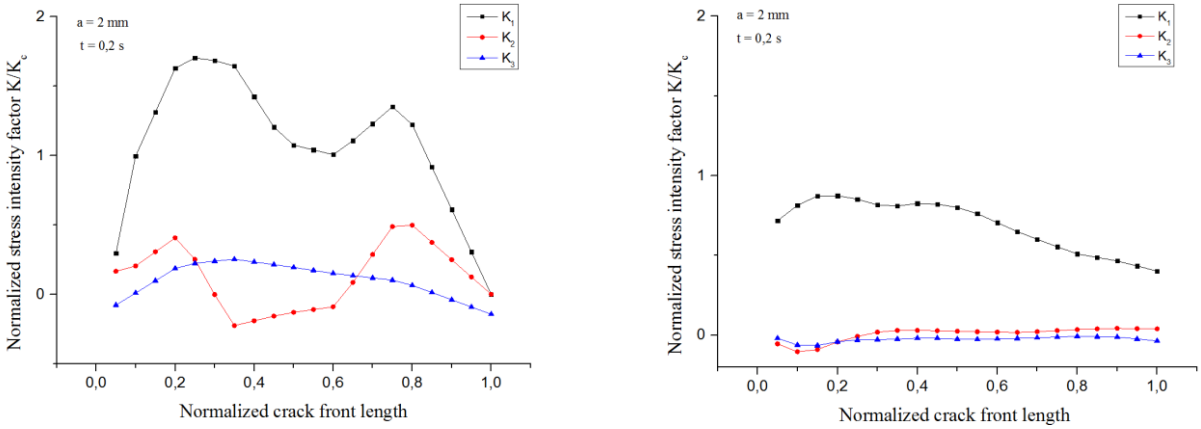

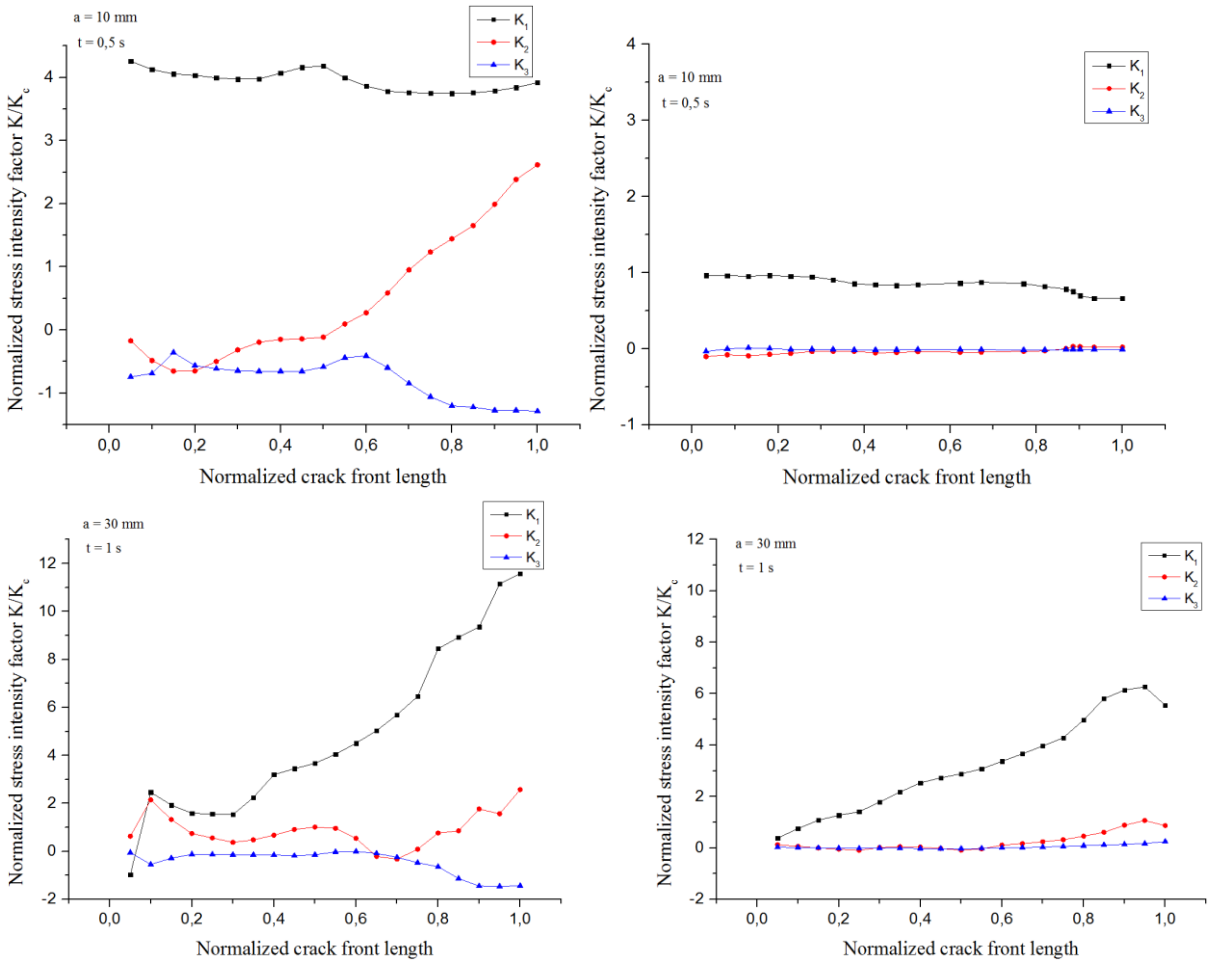

Fig. 11 stress intensity factor of two implanted.

Fig. 11 shows the stress intensity factors (KI, KII, KIII) as a function of the normalized distance of the crack forehead (contour) and has a length (2, 10 and 30 mm). The results of SIFs were taken at mode I. Because the SIFs at mode II and mode III were very small compared with at the value of modes I, the mode II and mode III values were not taken into account. In the model Osteal, the KI for the cracks in the different length, regardless, in the lateral to the medial part, the initiation of the crack propagates from the point (A) to point (B), started from a maximum value and gradually decreased to a minimum value, to the length of 10mm beyond this length this phenomenon is reversed. Same observation for model Charnley with significant values compared to the Osteal. That is to say, which means that the latter absorbs the load exerted by the patient.

7 Conclusion

In this paper, three selected methods (stress distribution, crack with X-FEM, stress intensity factor) are applied to compare of model Charnley and Osteal.

From the results, it can be concluded that:

(1) The difference of stress distributions in models The stress values in the bone femur are affected by the material, design and shape of the femoral stem.

In addition, the critical region is still predicted to be in the neck region (proximal part) for both hip prostheses with Charnley and Osteal stems.

(2) X-FEM shows advantages in modeling crack and provides reasonable results. To simulate cracking initiation and propagation was demonstrated to be effective for fracture analysis of bone.the well-known Charnley model. The Osteal prosthesis can have the longest life span X-FEM is recommended in modeling complicated cracks and structures.
(3) The KI values along the crack front showed oscillations, which may be due to the limitation of the enrichment function and limitations of the energy release integral implementation and the extraction domains. Mode I was the most dominant mode of loading crack in the bone cortical.
After a comparison between the present results of the two models confirm that the Osteal model of the hip prosthesis gives weak shear stresses in the bone cortical compared to the well-known Charnley model. The Osteal prosthesis can have the longest life span.

Références

[1] Beswick, A. and Blom, A. W. (2011). Bone graft substitutes in hip revision surgery: a comprehensive overview. Injury. 42 (Supplement 2), S40–S46
[2] Gao, L., Wang, F., Yang, P. and Jin, Z.(2009). Effect of 3D physiological loading and motion on elastohydrodynamic lubrication of metal-on-metal total hip replacements. Med. Eng. Phys. 31, 720–729.
[3] Harsha, A.P. and Joyce, T.J. (2013). Comparative wear tests of ultra-high molecular weight polyethylene and cross-linked polyethylene. Journal of Engineering in Medicine, 227(5), 600-608.
[4] El'Sheikh HF, MacDonald BJ, Hashmi MSJ. (2003). Finite element simulation of the hip joint during stumbling: A comparison between static and dynamic loading, J Mat Proc Tech143:249–255.
[5] S. SHANKAR and M. (2014). Mankandan dynamic contact analysis of total hip prosthesis during stumbling cycle. Journal of Mechanics in Medicine and Biology . Vol. 14, No. 3 .1450041.
[6] Moës N, Dolbow J, Belytschko T. (1999). A finite element method for crack growth without remeshing. Int J Numer Meth Engng;46:131–50.
[7] Sukumar N, Moës N, Moran N, Belytschko T. (2000). Extended finite element method for three-dimensional crack modelling. Int J Numer Meth Engng;48:1549–70.
[8] Adel, A. Abdel-Wahab.; Angelo, R.; Maligno, Vadim V. Silberschmidt. (2012). Micro-scale modelling of bovine cortical bone fracture: Analysis of crack propagation and microstructure using X-FEM. Computational Materials Science 52 128–135.
[9] Bonney H., Colston B.J., Goodman A.M., (2011). Regional variation in the mechanical properties of cortical bone from the porcine femur, Med. Eng. and Phys., 33, 4, 513-520.
[10] Simin, Li.; Adel Abdel-Wahab.; Emrah Demirci, Vadim V. Silberschmidt. (2013). Fracture process in cortical bone: X-FEM analysis of microstructured models. DOI 10.1007/978-3-319-04397-5_5.
[11] Budyn E, Hoc T. (2007). Multiple scale modeling of cortical bone fracture in tension using X-FEM. R E M N 16:213–236.
[12] Liu XC, Qin X, Du Z. (2010). Bone fracture analysis using the extended finite element method (XFEM) with abaqus. The 34th annual meeting of the American society of biomechanics. Brown University.
[13] Giner, E., Sukumar, N., Tarancón, J. E. and Fuenmayor, F. J. (2009). An Abaqus implementation of the extended finite element method. Eng Fract. Mech 76, 347–368.
[14] Bouiadjra, B. B., Belarbi, A., Benbarek, S., Achour, T. and Serier, B. (2007). FE analysis of the behaviour of microcracksin the cement mantle of reconstructed acetabulum in the total. hip prosthesis. Comp. Mater. Sci. 40, 485–491.

[15] Guian.Qian,V.F.González-Albuixech.Markus,Niffenegger.EugenioGiner. (2016). Comparison of KI calculation methods. Engineering Fracture Mechanics: 156.52–67.
[16] Bronzino, J.D. (2000). The Biomedical Engineering Handbook, volume 1. CRC Press.
[17] Kayabasi, O. and Erzincanli, F. 2006. Finite element modelling and analysis of a new cemented hip prosthesis. Advances in Engineering Software, 37(7), 477–483.
[18] Pyburn, E. and Goswami, T. (2004). Finite element analysis of femoral components paper III – hip joints. Materials and Design, 25(8), 705–713.
[19] Monif, M.M. (2012). Finite element study on the predicted equivalent stresses in the artificial hip joint. Journal of Biomedical Science and Engineering, 5, 43-51.
[20] Darwish, S.M. and Al-Samhan, A.M. (2009). Optimization of Artificial Hip Joint Parameters. Mat.-wiss. u. Werkstofftech, 40(3), 218-223.
[21] Bergmann, G. (2001). "HIP98", Free University, BerLin: ISBN 3-9807848-0-0.
[22] Bergmann G, Graichen F, Rohlmann A. (1993). Hip joint forces during walking and running, measured in two patients. J Biomech 26:969–990.
[23] Behrens, Bernd-Arno; Nolte, Ingo; Wefstaedt, Prick; Stukenborg-Colsman, Christina; Bouguecha, Anas.(2009). Numerical investigations on the strainadaptive bone remodelling in the periprosthetic femur: Inflience of the boundary conditions, BiomeEng, On line. 7.
[24] Ramaniraka, N.A., Rakotomanana, L.R. and Leyvraz, P.F. (2000). The fixation of cemented femoral component. Journal of Bone & Joint Surgery (Br), 82-B, 297-303.
[25] Abdelaziz, Y., Hamouine, A. (2008). A survey of the extended finite element. Comput. Struct. 86, 1141–1151.
[26] ABAQUS/Standard Version 6.13-1. (2013). Analysis user's manual, Dassault Systémes Simulia Corporation, Providence, RI, 2013. Hibbitt, Karlsson, Sorensen. Abaqus 6.13.1 Manual.
[27] Susan Mischinski and Ani Ural. (2013). Interaction of microstructure and microcrack growth in cortical bone: a finite element study" Computer Methods in Biomechanics and Biomedical Engineering, Vol. 16, No. 1, 81–94.
[28] Waisman, H.(2010). An analytical stiffness derivative extended finite element technique for extraction of crack tip Strain Energy Release Rates. Eng. Fract. Mech. 77, 3204–3215.
[29] Wyart, E., Duflot, M., Coulon, D., et al. (2008). Substructuring FE–XFE approaches applied to three-dimensional crack propagation. J. Comput. Appl. Math. 215, 626–638.